Journal of Materials Chemistry B

ROYAL SOCIETY OF CHEMISTRY

PAPER

View Article Online
View Journal

Cite this: DOI: 10.1039/d0tb00002g

Fibrous testing papers for fluorescence trace sensing and photodynamic destruction of antibiotic-resistant bacteria

Long Zhao,[ab] Yuan Liu,[a] Zhanlin Zhang,[a] Jiaojun Wei,[a] Songzhi Xie[a] and Xiaohong Li *[a]

Received 2nd January 2020,
Accepted 25th February 2020

DOI: 10.1039/d0tb00002g

rsc.li/materials-b

The increasing prevalence of antibiotic-resistant bacteria needs rapid identification and efficient destruction routes. This study proposes testing paper derived from electrospun fibrous mats and aggregation-induced emission (AIE) probes for trace sensing and simultaneous destruction of antibiotic-resistant *E. coli*. Aptamers are conjugated on fibers for selective capture of *E. coli*, and the capture capability can be regenerated *via* rinsing with salt solution. Hydroxyl tetraphenylethene (TPE) is linked with two cephalosporin molecules to construct TPE-Cep probes, and the fluorescence emission is turned on specifically in the presence of β-lactamase, which is a critical marker for screening resistant bacteria. Fibrous mats are lit up only in the presence of antibiotic-resistant bacteria, and the fluorescence intensity changes could be statistically fitted into an equation for quantitative analysis. Fibrous strips display apparent color changes from blue to green for a visual readout of bacterial levels, and the limit of detection (LOD) is much lower than those of previous paper substrates. In addition, the TPE-Cep probes could produce reactive oxygen species (ROS) under room light illumination to kill the captured bacteria. Thus, the integration of aptamer-grafted electrospun fibers and functional AIE probes provides potential for selective capture, trace imaging and photodynamic destruction of antibiotic-resistant bacteria.

Introduction

Infectious diseases have become a constant threat to human health, and bacterial infections cause over 300 million cases of severe illness each year. Antibiotic treatment has made significant contributions to infection control and remarkable reductions in the morbidity and mortality of infected patients. However, the bacterial resistance to antibiotics has increased dramatically over recent years due to the overuse of antibiotics in humans, veterinary medicine and the food industry.[1] The widespread presence of antibiotic-resistant bacteria is regarded as one of the most urgent challenges in human healthcare, animal breeding and environmental control. Thus, efficient and rapid identification of bacteria and drug-resistant strains plays important roles in monitoring epidemiology and directing effective risk management strategy. Especially in clinical practice, a real-time and reliable analysis of pathogenic bacteria is vital for preventing cross-infection and providing guidance for treatment protocols.[2]

A well-established gold standard for resistance detection is derived from bacterial growth in antibiotic-containing media.[3] Conventional bacterial cultures usually take 2–3 days or even longer to enrich samples for isolation and counting of pure colonies. These approaches are labor intensive, time consuming and less sensitive,[4] and usually cannot recognize a low population of antibiotic-resistant bacteria.[5] Given such deficiencies, attempts have been made in recent years for visual assessment of antibiotic resistance, enabling a rapid and direct observation of drug-resistant strains.[6] Among the resistance mechanisms, the disruption of antibiotic activities by β-lactamases has become the most significant and has an unavoidable consequence due to the wide and extended uses of β-lactam antibiotics. For example, penicillin, cephalosporin, monobactam and carbapenem exhibit antibacterial activities *via* interactions with penicillin binding proteins (PBPs) in the bacterial inner wall and then inhibiting cell wall synthesis. The expression of β-lactamases could destroy β-lactam structural moieties and diminish the antibacterial activities.[7] Thus, β-lactamase has been utilized as a critical marker for the detection and screening of resistant bacterial populations. Li *et al.* developed non-fluorescent probes containing a specific substrate of β-lactamase. The catalytic breakage of the

[a] *Key Laboratory of Advanced Technologies of Materials, Ministry of Education, School of Materials Science and Engineering, Southwest Jiaotong University, Chengdu 610031, P. R. China. E-mail: xhli@swjtu.edu.cn; Fax: +8628-87634649; Tel: +8628-87634068*

[b] *School of Bioscience and Technology, Chengdu Medical College, Chengdu 610031, P. R. China*

lactam ring caused the release of free fluorophores, and the fluorescence response was directly proportional to enzyme concentration.[8] However, the traditional imaging techniques face challenges in isolating specific strains and reporting a low level of resistant bacteria.[9]

Another challenge is the development of new antibacterial agents and alternative therapeutics to treat antibiotic-resistant infections. In contrast to target limitation and resistance generation for common antibiotics, photodynamic therapy (PDT) has become a promising alternative to deal with bacteria and prevent the generation of resistant bacteria.[10] Typically, bacteria are disrupted by reactive oxygen species (ROS) generated after light illumination of photosensitizers.[11] Jia *et al.* introduced a protoporphyrin photosensitizer and quaternary ammonium salt groups into cellulose, and ROS was produced under light irradiation for the effective destruction of drug-resistant bacterial strains.[12] Lin *et al.* developed silica nanoparticles with loaded chlorin e6, and singlet oxygen was continuously generated under light illumination to inhibit bacterial growth.[13] Thus, the integration of diagnostic and therapeutic capabilities within activatable probes should provide great potential in the simultaneous imaging and photodynamic ablation of bacteria.[14] But poor photostability and low bacterial affinity of conventional fluorescent photosensitizers hinder their successful application in the real-time detection and simultaneous treatment of bacterial infections.[15] Furthermore, most of the fluorescent probes and photosensitizers are extremely hydrophobic and have strong π–π stacking interactions, resulting in aggregation-induced quenching (ACQ). The quenched emission and reduced ROS generation decrease the labeling and antibacterial capabilities, but little progress has been made in circumventing the ACQ profiles of photosensitizers.[16,17] Alternatively, probes with aggregation-induced emission (AIE) characteristics, such as derivatives from propeller-like tetraphenylethene (TPE) molecules, have shown high fluorescence emission and ROS generation in an aggregation state.[18] The light-induced ROS generation from some AIE luminogens has been used to kill cancer cells and bacteria, but challenges remain in imaging and distinguishing antibiotic-resistant bacteria from susceptible bacteria.[19]

In the current study, electrospun fibrous strips were integrated with capture ligands and AIE probes for selective sensing and photodynamic destruction of antibiotic-resistant bacteria. *E. coli*, as a biomarker of environmental contamination, is one type of commensal bacteria in the gastrointestinal tract of humans and many animals. Resistant *E. coli* makes up the majority of bacterial pathogens commonly associated with antimicrobial resistance and survives almost any individual antibiotic treatment.[20] Electrospun fibrous mats have high specific surface areas and facilitate high sensitivity and rapid response for sensing applications due to the easy accessibility of functional moieties and the increase in the reaction rates.[21] In our previous study, TPE and mannose were conjugated on electrospun fibers, and the mannose grafts established specific interactions with FimH proteins from the fimbriae of *E. coli*. The AIE feature of TPE grafts led to an obvious fluorescence "turn-on" of the fibrous mats.[22] In the current study, aptamer ligands are designed for specific recognition of *E. coli* and exhibit advantages over the commonly used antibodies due to their low cost, few batch-to-batch variations and high stability in a wide range of temperatures and pH values.[23] As shown in Scheme 1, electrospun blend fibers of poly(styrene-*co*-maleic anhydride) and polystyrene (PSMA/PS) with grafted *E. coli*-specific aptamers (Apt-*g*-PSMA/PS) were constructed for bacterial capture, followed by utilization of AIE probes for recognizing and destroying antibiotic-resistant strains. The AIE probes consisted of TPE cores and two terminal cephalosporin molecules (TPE-Cep) to promote water solubility. After capture by *E. coli*, the TPE-Cep probes were only cleaved by endogenous β-lactamase in penicillin-resistant bacteria to yield TPE with two hydroxyl groups (TPE-OH), which

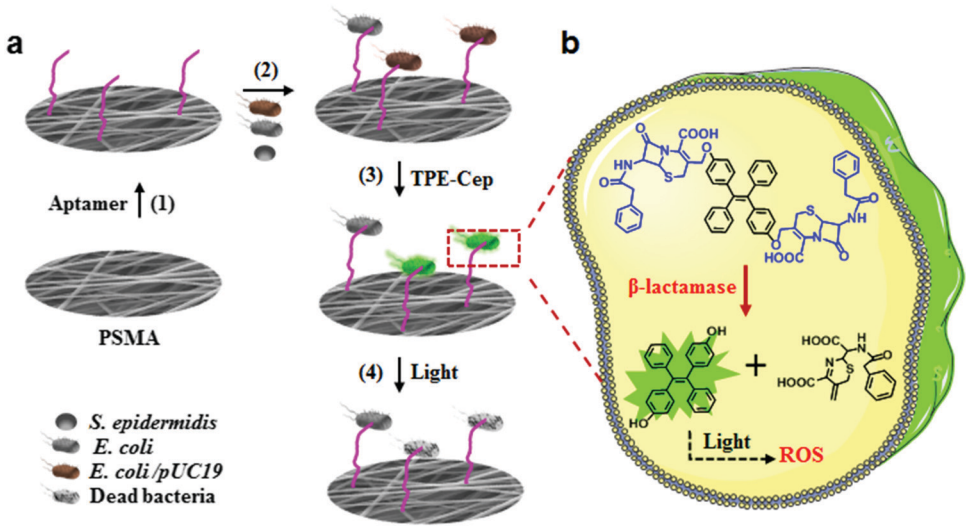

Scheme 1 (a) Schematic drawing of bacterial capture and destruction on fibrous mats. Aptamers are grafted on PSMA/PS fibers (1), followed by specific capture of *E. coli*/*pUC19* and *E. coli* (2). TPE-Cep probes are used to light up *E. coli*/*pUC19* only (3), followed by destruction of *E. coli*/*pUC19* under room light illumination (4). (b) Schematic drawing of bacterial sensing and destroying mechanism. TPE-Cep probes are recognized and cleaved into fluorescent TPE-OH by endogenous β-lactamase in antibiotic-resistant bacteria, followed by light irradiation to produce ROS for bacterial destruction.

formed aggregates and emitted fluorescence immediately. Owing to the AIE activity and excellent water dispersion of TPE-Cep probes, the imaging process of resistant bacteria can be simplified without washing. As a photosensitizer, the released TPE-OH could produce ROS under light illumination to destroy bacteria. Thus, the TPE-Cep probes demonstrate multiple functions toward exactly imaging and image-guided PDT of antibiotic-resistant bacteria.

Experimental section

Materials

PSMA (M_w: 170 kDa, maleic anhydride content: 14.8 wt%) and PS (M_w: 400 kDa) were obtained from Shanghai Zhaocheng Scientific Development Corp (Shanghai, China). Penicillin, 4-methoxybenzyl 3-chloromethyl-7-(2-phenylacetamido)-3-cephem-4-carboxylate (GCLE), bovine serum albumin (BSA), trypsin, dichlorofluorescein diacetate (DCFH-DA), β-lactamase, lysozyme, esterase, hydroxybenzophenone and potassium clavulanate (PCA) were procured from Sigma (St Louis, MO). Sodium iodide, anisole, trifluoroacetic acid, and toluidine blue O (TBO) were purchased from Tianjin Heowns Biochemical Technology Co., Ltd (Tianjin, China). The sequences for 3′-amino-modified *E. coli*-specific aptamer were as follows: 5′-GCA ATG GTA CGG TAC TTC CCC ATG AGT GTT GTG AAA TGT TGG GAC ACT AGG TGG CAT AGA GCC GCA AAA GTG CAC GCT ACT TTG CTA A-3′, which was obtained from Sangon Biotech Co., Ltd (Shanghai, China). *S. epidermidis* (ATCC 12228) and *P. aeruginosa* (ATCC 35032) were purchased from the American Type Culture Collection (Rockville, MD). *Escherichia coli* JM109 (*E. coli*) and penicillin-resistant *E. coli* (*E. coli*/*pUC19*) were donated by Xiamen University (Xiamen, China). All other chemicals were of analytical grade and obtained from Changzheng Regents Company (Chengdu, China), unless otherwise indicated.

Synthesis of TPE-Cep

Fig. 1a shows the preparation process of TPE-Cep probes by conjugation of TPE-OH and GCLE, followed by the removal of *p*-methoxybenzyl protection groups. TPE-OH was synthesized from 4-hydroxybenzophenone *via* the McMurry reaction as described previously.[24] Briefly, 1.64 g of Zn powder (25.0 mmol) and 1.56 mL of $TiCl_4$ (14.0 mmol) were mixed in 50 mL of dry tetrahydrofuran (THF) and then refluxed for 2 h. After the addition of dry THF (30 mL) containing 1.98 g of 4-hydroxybenzophenone (10.0 mmol), the mixture was refluxed for 4 h and incubated with 10% aqueous K_2CO_3 solution. The reaction mixture was vacuum-filtered to remove insoluble materials, and the aqueous layer was

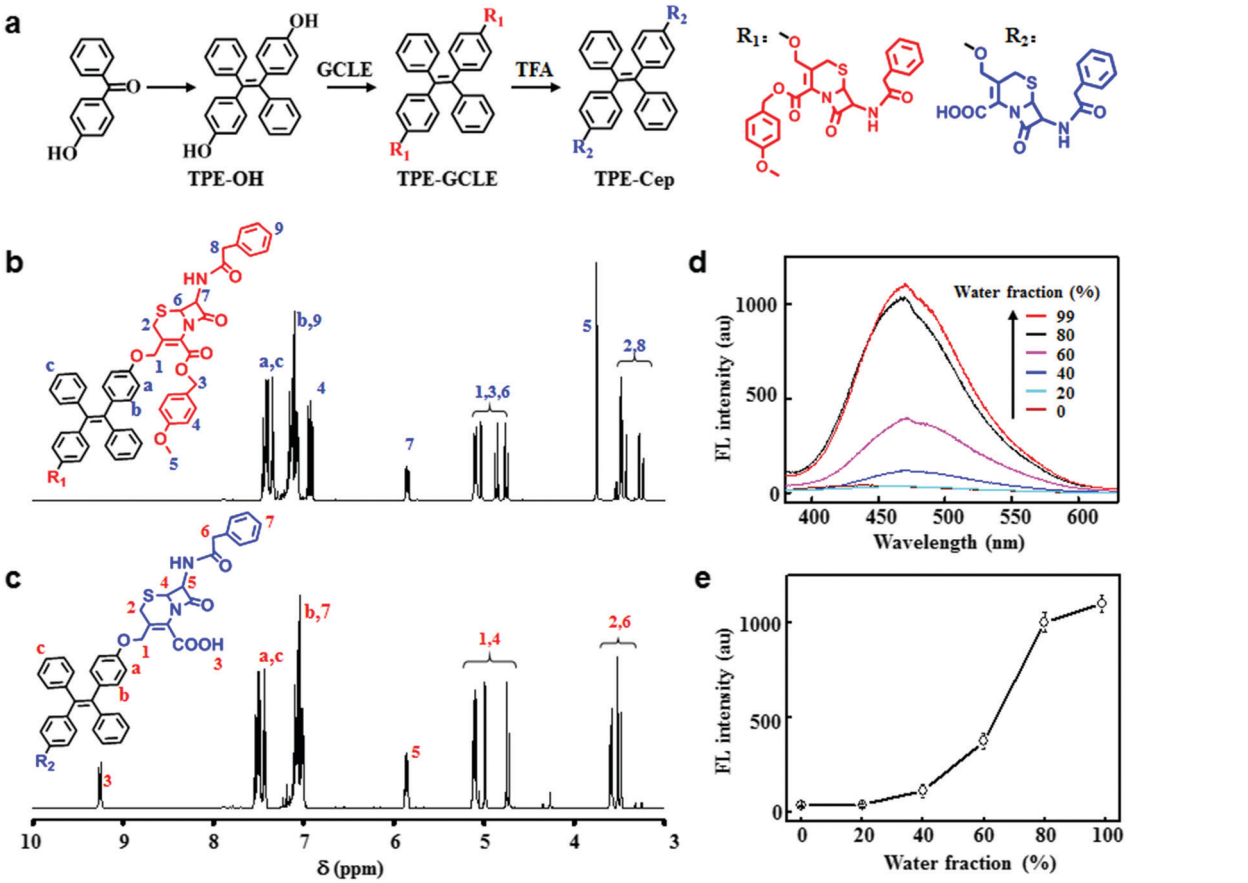

Fig. 1 (a) Synthetic route for TPE-Cep. (b) ^{1}H NMR spectra of TPE-GCLE and (c) TPE-Cep. (d) Fluorescence spectra of TPE-GCLE in DMSO/water mixtures of different water fractions up to 99%. (e) Fluorescence intensity change of TPE-GCLE at 466 nm after incubation in DMSO/water mixtures with different water fractions (n = 3).

extracted with ethyl acetate. The organic fractions were water-washed, Na_2SO_4-dried, and then vacuum-evaporated, followed by separation using silica gel to give TPE-OH. A yield of 56% was obtained. The ^{1}H NMR spectrum was recorded using a Bruker AM 400 apparatus, using tetramethylsilane (TMS) as the internal reference. ^{1}H NMR ($CDCl_3$, ppm): δ 7.06 (d, 8H), 6.88 (d, 2H), and 6.57 (d, 8H).

GCLE was conjugated on TPE-OH *via* esterification as described previously.[8] Briefly, GCLE (1.46 g, 3.0 mmol), sodium iodide (0.43 g, 3.0 mmol), and K_2CO_3 (0.40 g, 1.3 mmol) were mixed in 8 mL of acetonitrile for 15 min, followed by dropwise addition of TPE-OH (0.36 g, 1.0 mmol) in 4 mL of acetonitrile. After vigorous stirring for 1 h, the solvent was removed by vacuum evaporation, and the crude product was dissolved in a mixture of water (10 mL) and ethyl acetate (15 mL). The organic fractions were washed with 10% aqueous $Na_2S_2O_3$ solution and dried with Na_2SO_4, followed by separation using silica gel to give TPE-GCLE (0.37 g, 30% yield) as a yellow solid. ^{1}H NMR ($CDCl_3$, ppm): δ 7.33–7.46 (m, 14H), 7.06–7.17 (m, 18H), 6.90–6.96 (m, 4H), 5.80 (m, 1H), 5.11 (d, 2H), 5.05 (d, 1H), 4.86 (d, 1H), 4.77 (d, 1H), 3.75 (s, 3H), 3.57 (d, 2H), 3.45 (d, 1H), and 3.27 (d, 1H) (Fig. 1b).

TPE-GCLE (148 mg, 0.12 mmol) was dissolved in 4 mL of dichloromethane at 0 °C under argon, followed by adding 0.10 mL of anisole and 0.50 mL of trifluoroacetic acid. After vigorous stirring for 1 h, the solvent was removed by vacuum evaporation, and the residue was separated using silica gel to give TPE-Cep (52 mg, 42% yield) as a yellow solid. ^{1}H NMR ($CDCl_3$, ppm): δ 9.19 (d, 1H), 7.41–7.55 (m, 14H), 6.98–7.13 (m, 14H), 5.80 (m, 1H), 5.09 (d, 1H), 4.98 (d, 1H), 4.73 (d, 1H), 3.62 (d, 2H), and 3.49 (d, 2H) (Fig. 1c).

Characterization of TPE-Cep

The AIE properties of TPE-GCLE were determined from the changes in fluorescence emissions in dimethyl sulfoxide (DMSO)/water mixtures.[25] Briefly, TPE-GCLE was dissolved in DMSO at a concentration of 1 mM, and water was added dropwise with fractions from 0 to 99% under vigorous stirring. The emission spectra of the resulting solutions or suspensions were measured using a fluorescence spectrophotometer (Hitachi F-7000, Japan) at the excitation/emission wavelengths of 365/466 nm.

The sensitivity of TPE-Cep probes was detected from the fluorescence emission change in the presence of β-lactamase. Briefly, a TPE-Cep solution (3 mM) in phosphate buffered saline (PBS, pH 7.4) was mixed with β-lactamase solution (3.0 U mL^{-1}). After incubation at 37 °C for 20 min, the reaction mixtures were measured using a fluorescence spectrophotometer as above and photographed under a 365 nm UV lamp. The inhibition assay of enzyme activity was performed in the presence of PCA.[26] Briefly, PCA solution (1, 5, and 10 μM) was premixed with β-lactamase (5.0 U mL^{-1}) for 10 min at 37 °C, followed by addition of TPE-Cep probes (2 mM). After vigorous shaking for 20 min, the fluorescence intensity of the reaction mixtures was measured immediately using a fluorescence spectrophotometer as above. To investigate the specific interactions between β-lactamase and β-lactam ring, β-lactamase (5.0 U mL^{-1}), penicillin (5, 10, and 20 μM) and TPE-Cep probes (2 mM) were mixed in aqueous solutions for 20 min, followed by measuring the fluorescence intensities as above.[26] The specificity of the TPE-Cep probes was also investigated in the presence of other substances, such as proteins (BSA, trypsin, lysozyme and esterase), inorganic salts ($CaCl_2$ and $CuSO_4$), and organic molecules (glucose).

Preparation and modification of electrospun fibers

Blend fibers of PSMA and PS were prepared by electrospinning, and aptamers were grafted on the fibers *via* amidation reaction (Scheme 1a). Briefly, PSMA and PS were mixed with different ratios of THF/acetone/dimethylformamide (5 : 3 : 2, v/v/v). Electrospinning was conducted under a fixed electric field of 20 kV/15 cm, and the flow rate of polymer solution was 10 mL h^{-1}.[27] The collected PSMA/PS fibers were immersed in Tris–HCl buffer (10 mM, pH 7.4) containing 3′-amino-modified *E. coli*-specific aptamer (1 μM), followed by incubation at room temperature for 3 h to obtain Apt-*g*-PSMA/PS fibers. The reaction media were retrieved and precipitated with ethanol, and the aptamer concentration was measured using an ultraviolet-visible (UV-Vis) spectrophotometer (UV-2550, Shimadzu, Japan) to determine the grafting content on the fibers.[28] The resulting fibers were treated with 100 mM ethanolamine for 1 h to block unoccupied anhydride groups, followed by washing with Tris–HCl buffer and drying under a N_2 stream.[28]

Characterization of electrospun fibers

Scanning electron microscopy (SEM; JSM-7800F, JEOL, Japan) was used to observe the morphologies of the electrospun fibers, and the fiber size, pore size and the porosity of fibrous mats were determined from the SEM images.[29] The hydrophilicity of fibrous mats was determined from the water contact angles (WCAs) using a Kruss GmbH DSA100 Mk 2 goniometer (Hamburg, Germany). The chemical compositions of fibers were analysed using X-ray photoelectron spectroscopy (XPS, XSAM800, Kratos Ltd, UK), which was operated between 50 and 1300 eV with an energy step of 0.5 eV using a pass energy of 300 eV. The density of the anhydride groups on the fiber surface was measured *via* the TBO binding method after reaction with ethanolamine and conversion into carboxyl groups.[30] Briefly, the fibers were immersed in 100 mM ethanolamine at 25 °C for 1 h, and then incubated in TBO solution (0.50 mM), which was adjusted to pH 10 with 0.10 mM NaOH. After constant agitation for 5 h at room temperature, the retrieved fibers were intensively washed with 0.1 mM NaOH solution to remove the noncomplexed TBO. The resulting fibers were mixed in acetic acid solution (50%) for 10 min to desorb TBO, which was detected using a UV-Vis spectrophotometer at 633 nm.

Bacterial capture on fibrous mats

The bacterial capture on fibrous mats was examined using *E. coli*/*pUC19* as a drug-resistant bacterial model, and using *E. coli*, *S. epidermidis* and *P. aeruginosa* as controls. Bacteria were cultured in Luria-Bertani (LB) media for 12 h and diluted with PBS. Fibrous mats were cut into round discs with a diameter of 10 mm, followed by incubation with 1 mL of bacterial suspension in PBS (10^5 CFU mL^{-1}). Fibrous mats were intensively rinsed with

PBS, and the bacterial concentration in the washing solution was determined using a UV-Vis spectrophotometer at 600 nm (OD600) to calculate the amount of bacteria captured. The bacteria-loaded fibrous mats were observed by SEM as above after fixation in 4% paraformaldehyde and lyophilization.

Bacterial detection and killing efficiency

The bacteria-captured fibers were incubated with TPE-Cep probes at a concentration of 1.0 mg mL^{-1} in the dark for 20 min. After PBS washing, the fibrous mats were detected using a fluorescence spectrophotometer at the excitation wavelengths of 365 nm and photographed under a 365 nm UV lamp. In addition, the bacteria-captured fibers were treated with penicillin solution (1 μM) for 20 min before incubation with TPE-Cep probes. To regenerate the aptamer sensors, the bacteria-captured fibrous mats were rinsed using 2 M NaCl at 60 °C.[31] The regenerated fibrous mats were used to capture and detect bacteria, and the fluorescence spectra were recorded as above. The detection and regeneration processes were repeated for 5 cycles. The ROS levels in the bacterial cells were measured after incubation with DCFH-DA as described previously with some modifications.[32] Briefly, TPE-Cep probe-stained fibers with captured bacteria were resuspended in PBS containing 30 μg mL^{-1} DCFH-DA at 37 °C for 30 min. The fibers were collected and exposed to room light for 10 min, while the control groups were kept in the dark. The fluorescence intensity was measured at the excitation/emission wavelengths of 485/520 nm. The morphology of bacteria was observed by SEM as above after fixation in 4% paraformaldehyde and lyophilization.

Statistical analysis

The statistical significance of the data obtained was analyzed by Student's *t*-test. Data are expressed as mean ± standard deviation (S.D.). Probability values of $p < 0.05$ were interpreted as denoting statistical significance.

Results and discussion

Characterization of TPE-Cep probes

TPE-GCLE was prepared by coupling GCLE on TPE-OH, which was synthesized *via* McMurry reaction between two molecules of 4-hydroxybenzophenone (Fig. 1a). As shown in the ^{1}H NMR spectra, the disappearance of peaks at 5.11 (d, 2H) and 3.75 ppm (s, 3H) indicated the removal of *p*-methoxybenzyl groups from TPE-GCLE (Fig. 1b), while the peak at 9.19 ppm (d, 1H) belonged to the carboxyl groups of the resulting TPE-Cep (Fig. 1c). The AIE properties of TPE-GCLE were measured from fluorescence changes in DMSO after the addition of water.[25] Fig. 1d shows the fluorescence spectra of TPE-GCLE, indicating significant increases in the fluorescence intensities with increasing water fractions. DMSO is a good solvent for TPE-GCLE, and the addition of water induced aggregation and then fluorescence emission. As shown in Fig. 1e, the fluorescence emission of TPE-GCLE became visible when the water fractions were over 40%. When the water fractions increased from 40% to 99%, the fluorescence intensities of TPE-GCLE increased by around 17 fold, indicating the maintenance of AIE activities.

Fluorescence response of TPE-Cep probes to β-lactamase

The β-lactam of cephalosporin was subjected to specific hydrolysis by β-lactamase, and cephalosporin could be used as a substrate for β-lactamase recognition.[8] Fig. 2a shows the fluorescence intensities of TPE-Cep probes upon the addition of β-lactamase in PBS. The cephalosporin structure in the TPE-Cep probes could be recognized and hydrolyzed by β-lactamase and subsequently release TPE-OH,

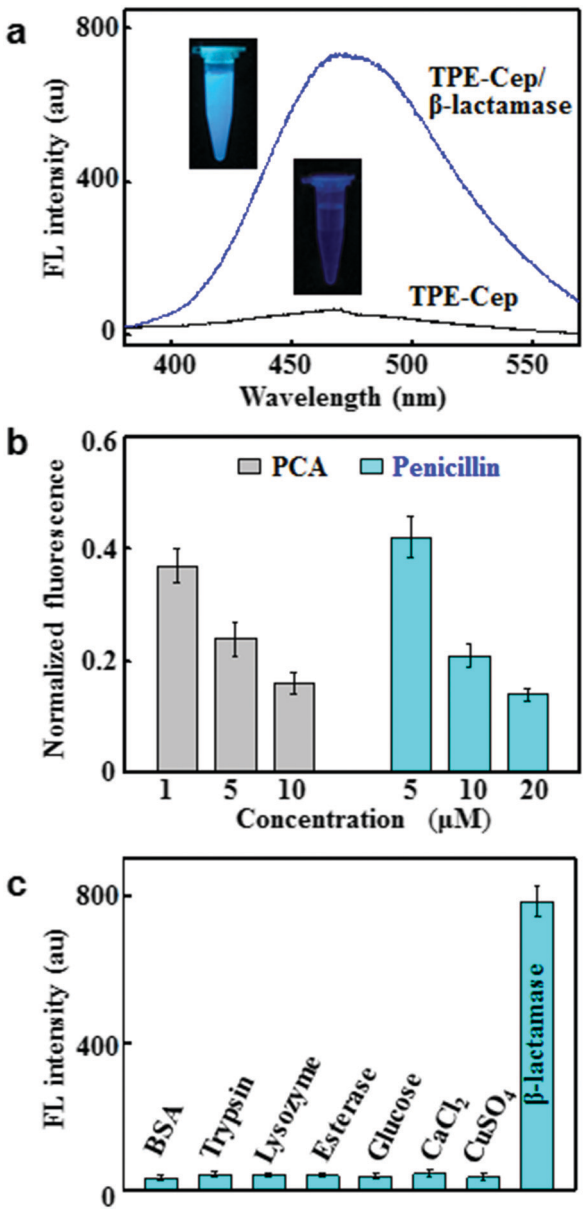

Fig. 2 (a) Fluorescence spectra of TPE-Cep in PBS and in the presence of β-lactamase. Insets are photographs of the solutions under illumination obtained by using a hand-held ultraviolet lamp. (b) Fluorescence intensities of TPE-Cep after incubation with β-lactamase in the presence of PCA and penicillin at different concentrations (n = 3). (c) Fluorescence intensities of TPE-Cep probes in the presence of β-lactamase, BSA, trypsin, lysozyme, esterase, glucose, $CaCl_2$ and $CuSO_4$ (n = 3).

which formed aggregates immediately in PBS and emitted fluorescence at 468 nm. As shown in the inset of Fig. 2a, under UV illumination, the fluorescence emission of TPE-Cep was observed in the presence of β-lactamase.

To verify that the fluorescence turn-on resulted from the hydrolysis of cephalosporin, PCA was added as an inhibitor of β-lactamase. As shown in Fig. 2b, there were decreases of around 63%, 76% and 84% in the fluorescence intensities after the addition of 1, 5 and 10 μM PCA, respectively, due to the irreversible binding with the active site of β-lactamase.[33] In addition, penicillin could interrupt the specific interaction between β-lactamase and TPE-Cep, due to the competitive binding with β-lactamase.[26] As expected, the fluorescence emission of the probes was much weaker with the increase of penicillin concentrations (Fig. 2b). The above data indicated that the fluorescence turn-on was mainly attributed to the specific recognition of TPE-Cep and hydrolysis by β-lactamase into its highly fluorescent counterpart TPE-OH. The specificity of TPE-Cep probes to β-lactamase was evaluated from the fluorescence response in the presence of various interferences. As shown in Fig. 2c, there was no significant increase in the fluorescence intensities of TPE-Cep probes after incubation with proteins BSA, enzymes (trypsin, lysozyme and esterase), inorganic salts ($CaCl_2$ and $CuSO_4$), and organic molecules (glucose). Thus, TPE-Cep could be an effective and specific probe for the detection of β-lactamase from antibiotic-resistant bacteria.

Characterization of Apt-*g*-PSMA/PS fibrous mats

Fig. 3a shows typical SEM images of PSMA/PS and Apt-*g*-PSMA/PS fibers containing 50% PSMA. The aptamer grafting maintained the integral fibrous morphology and randomly arrayed feature. The average sizes of pristine and aptamer-grafted fibers were 1.38 and 1.84 μm, respectively, providing high specific surface areas for bacterial binding. PSMA/PS fibers showed a hydrophobic surface with a WCA of around 126°, and the aptamer grafts on the fiber surface significantly increased the hydrophilicity (38°). The increase in the hydrophilicity of fibers led to water swelling of the fiber matrix and a significant increase in size. In addition, the aptamer grafting led to a decrease in the average pore sizes from 13.5 to 7.7 μm and porosities from 93% to 82%. Fig. 3b shows the typical XPS profiles of the fibers. Additional N1s (400 eV) and P2p peaks (135 eV) appeared, due to amidation between terminal amino groups of aptamer and anhydride groups on the fiber surface.

PSMA was mixed with PS in different fractions to adjust the densities of anhydride groups and aptamer grafts on the fiber surface. Fig. 3c shows the densities of anhydride groups on the fiber surface, determined after transformation into carboxyl groups. The increase in PSMA fractions from 40% to 60% led to an almost linear increase in anhydride group densities from 2.1 to 11.4 mmol mg^{-1} fibers. The grafting amount of aptamers on fibers increased with the PSMA contents and the increase of aptamer densities was consistent with that of the anhydride groups on the fiber surface (Fig. 3c), suggesting the sufficient conjugation of aptamers on fibers.

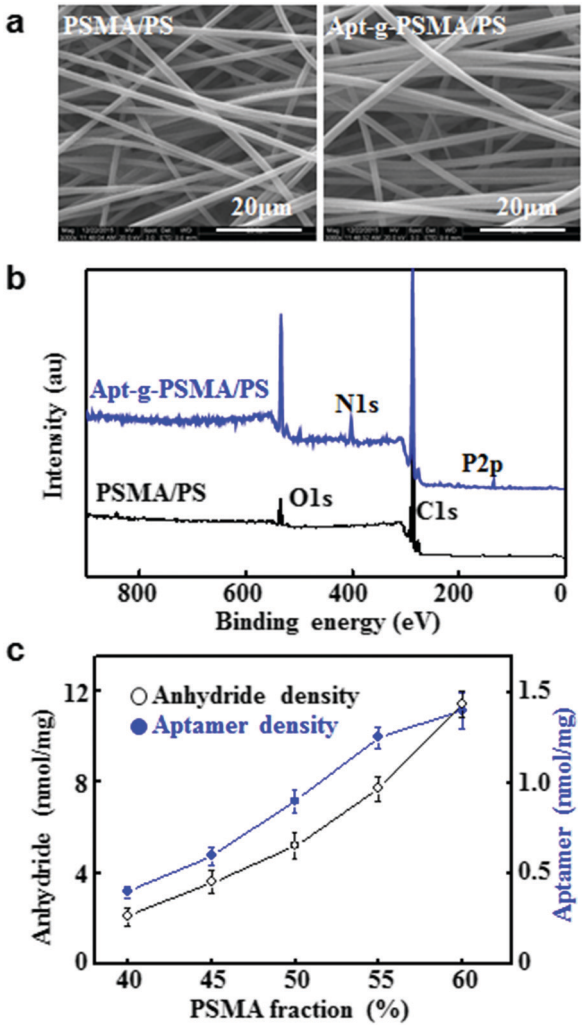

Fig. 3 (a) Typical SEM images and (b) XPS spectra of electrospun PSMA/PS and Apt-*g*-PSMA/PS fibers. (c) Densities of anhydride groups and aptamers on the surface of fibers with different PSMA fractions (n = 3).

Bacterial capture on fibers

Fig. 4a summarizes the amount of bacteria captured on fibrous mats after incubation with *E. coli*/*pUC19* suspensions. There was a rapid increase in the bacterial amount during the early incubation stage and no more increase after incubation for 50 min, which was set as the incubation time during the following tests. Fig. 4b shows the amount of *E. coli*/*pUC19* captured by fibers, indicating significantly higher capture efficiency by fibers with higher aptamer levels ($p < 0.05$). The amount of captured bacteria indicated no significant increase when the PSMA fractions in fibers increased to over 50%. It was indicated that the reaction between bacteria and aptamer grafts reached saturation when the graft density of aptamers increased to 0.9 nmol mg^{-1}, which was used in the following investigation. Fig. 4c shows a typical SEM image of the bacteria-captured fibers, displaying the abundant existence of bacteria on fibers. In order to confirm the capture specificity of aptamers to *E. coli*, *S. epidermidis* and *P. aeruginosa* were used as controls.[34] As shown in Fig. 4d, compared with the efficient capture of *E. coli*/*pUC19*

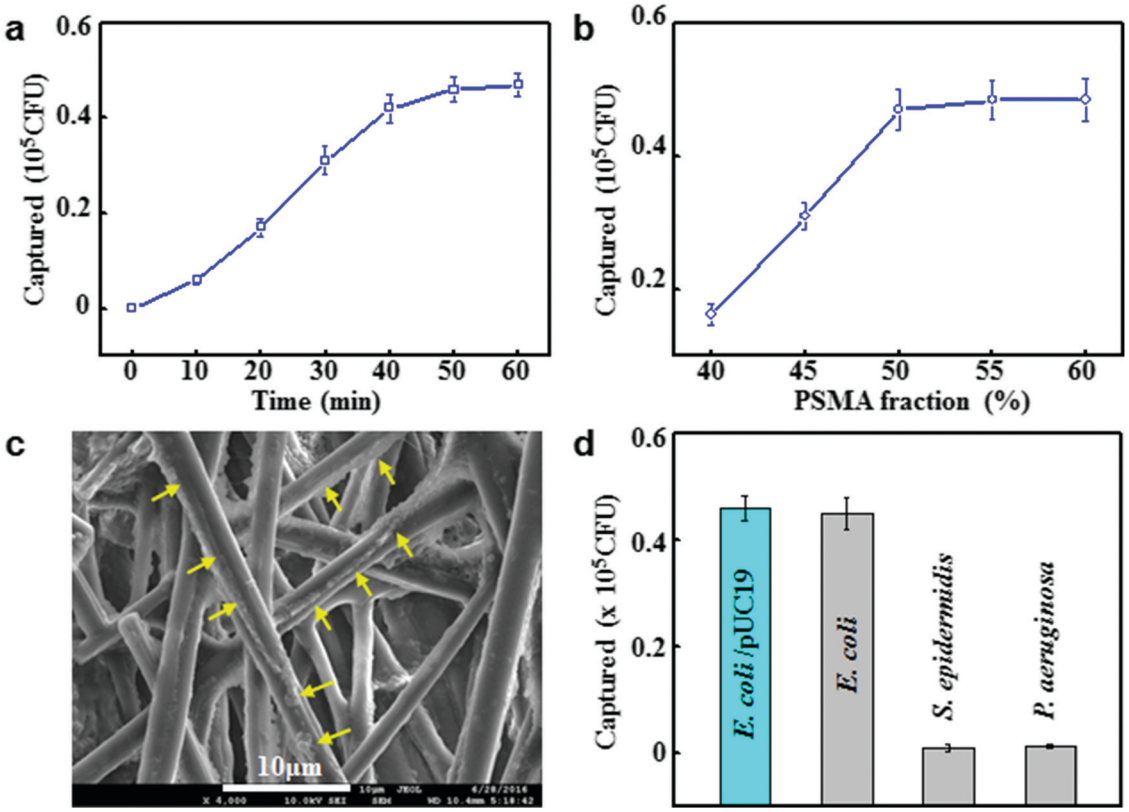

Fig. 4 (a) Bacterial capture amount after incubation for up to 60 min with *E. coli/pUC19* at 10^5 CFU mL^{-1} (n = 3). (b) Bacterial capture amount by fibers with different PSMA fractions after incubation with *E. coli/pUC19* at 10^5 CFU mL^{-1} for 50 min (n = 3). (c) Typical SEM morphology of bacteria-captured fibrous mats. Arrows indicate the captured bacteria. (d) Bacterial capture amount after incubation with *E. coli/pUC19, E. coli, S. epidermidis* and *P. aeruginosa* at 10^5 CFU mL^{-1} for 50 min (n = 3).

and *E. coli*, there was no apparent capture of *S. epidermidis* and *P. aeruginosa* on the fiber surface.

Bacteria detection with TPE-Cep probes

The expression of β-lactamase is responsible for the resistance of *E. coli/pUC19* to β-lactam antibiotics.[35] As shown in Fig. 2, the TPE-Cep probes showed high sensitivity to β-lactamase and strong fluorescence emission. We then investigated their applicability in the fluorescence detection of *E. coli/pUC19*. Fig. 5a shows the fluorescence intensities of captured bacteria on fibers after incubation with the TPE-Cep probes. As expected, fibers with captured *E. coli/pUC19* showed high fluorescence intensities, while almost no fluorescence emission was observed for fibers after incubation with *S. epidermidis* and *P. aeruginosa*. Although the antibiotic-susceptible *E. coli* strain could not express β-lactamase, fibers with captured *E. coli* showed a weak fluorescence intensity after treatment with the TPE-Cep probes. In order to clarify the fluorescence emission, fibers with captured *E. coli* strain were treated with free penicillin before incubation with the TPE-Cep probes. As shown in Fig. 5b, the treatment with penicillin led to no remarkable change in the emission intensities of fibers after capture of *E. coli/pUC19* at 10^4 and 10^5 CFU mL^{-1} ($p > 0.05$), which was attributed to the high-level expression of β-lactamase in this strain. However, significantly lower fluorescence intensities were observed for *E. coli*-captured fibers after penicillin treatment ($p < 0.05$). As is known, β-lactams target peptidoglycan synthesis in bacteria *via* inactivating the transpeptidase activity of PBPs.[36] Then, the cephalosporin moieties in the TPE-Cep probes could recognize PBPs on the periplasmic surface of the cytoplasmic membrane of bacteria,[35] and the specific binding between them led to weak fluorescence due to the AIE effect. The addition of penicillin would lead to the occupation of the PBP sites, leading to no significant fluorescence emission after incubation with the TPE-Cep probes. Thus, in the case of bacterial mixtures, the determination of *E. coli/pUC19* could be performed after treatment with both TPE-Cep probes and penicillin, and the fluorescence difference with and without penicillin addition could reflect the presence of *E. coli*.

Fig. 5c shows typical fluorescence spectra of fibers in response to bacteria levels up to 10^6 CFU mL^{-1}. As summarized in Fig. 5d, the fluorescence intensity of the bacteria-captured fibers progressively increased as the bacterial concentrations increased up to 10^5 CFU mL^{-1}. The fluorescence intensity of fibrous mats was drafted against *E. coli/pUC19* levels and expressed by the equation:

$$Y = 26X^{0.28} \ (R^2 = 0.992)$$

where Y represents the fluorescence intensity and X is the bacterial concentration (0–10^5 CFU mL^{-1}). Thus, the bacterial levels can be determined from the fluorescence emissions according to the above equation. On the basis of the signal-to-noise ratio of 3,[37] the limit of detection (LOD) of the current assay was 60 CFU mL^{-1},

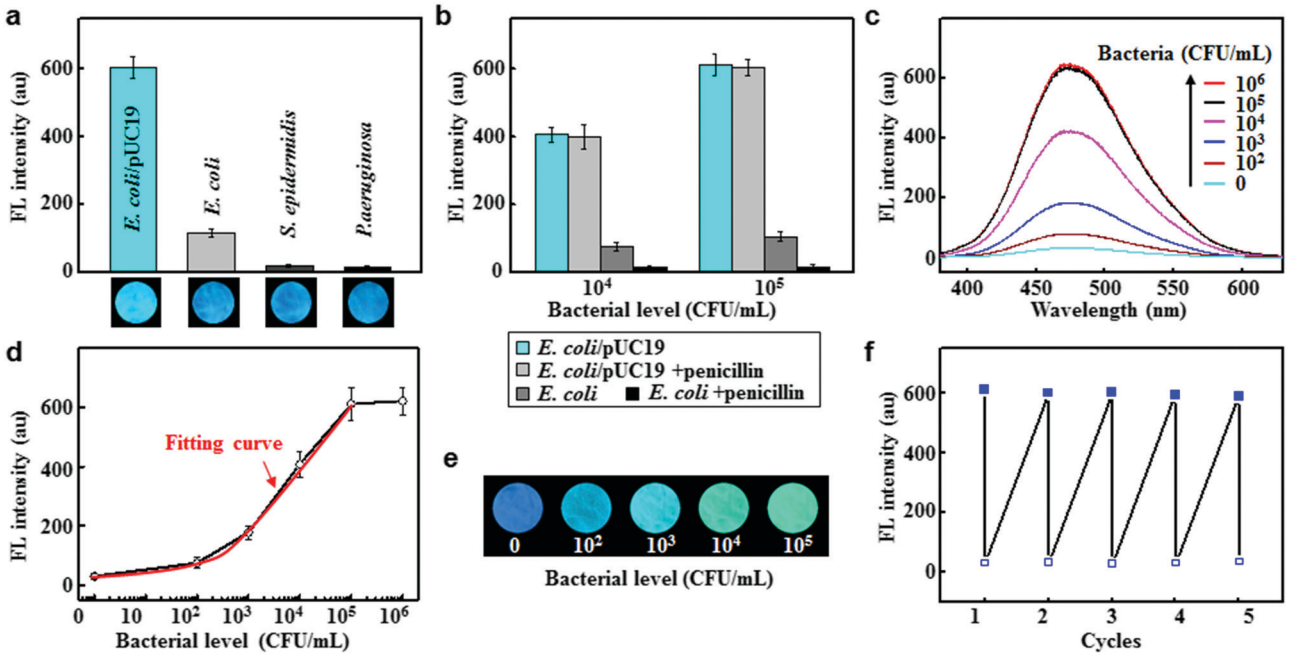

Fig. 5 (a) Fluorescence intensities of *E. coli*/*pUC19*, *E. coli*, *S. epidermidis* and *P. aeruginosa* captured on fibers after incubation with TPE-Cep probes (n = 3). (b) Fluorescence intensities of captured *E. coli*/*pUC19* and *E. coli* (10^4 and 10^5 CFU mL^{-1}) after incubation with TPE-Cep probes in the absence and presence of penicillin (n = 3). (c) Fluorescence spectra and (d) intensities of fibrous mats after incubation with *E. coli*/*pUC19* at different concentrations, followed by treatment with TPE-Cep probes (n = 3). (e) Color strips of fibrous mats in the presence of *E. coli*/*pUC19* at different concentrations taken at 365 nm under illumination of a hand-held UV lamp. (f) Fluorescence intensity of bacteria captured on fibers after TPE-Cep treatment for different cycles (n = 3).

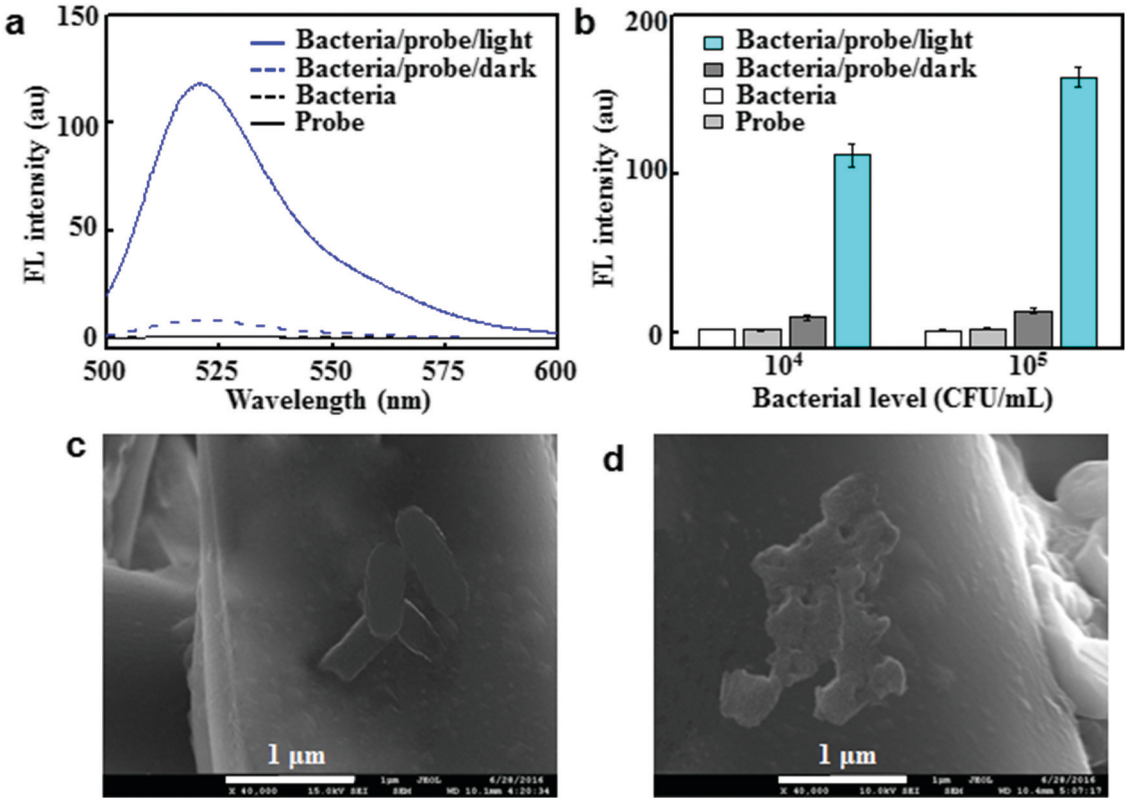

Fig. 6 (a) Fluorescence spectra of DCFH-DA in the presence of captured *E. coli*/*pUC19*, TPE-Cep probes and the mixtures in the dark and under light illumination. (b) Fluorescence intensity of DCFH-DA in the presence of captured *bacteria*, TPE-Cep probes and the mixtures in the dark and under room light illumination after incubation with *E. coli*/*pUC19* of 10^4 and 10^5 CFU mL^{-1} (n = 3). (c) SEM images of *E. coli*/*pUC19* captured after incubation with TPE-Cep probes in the dark and (d) under light irradiation.

which was lower than that of previous assays on paper substrates. Naik *et al.* integrated thermal lysis and DNA amplification from bacteria into a single reaction step for *E. coli* assay, indicating a LOD of 100 CFU mL^{-1}.[38] In addition, a color strip was constructed to achieve a visual readout of bacterial levels. As shown in Fig. 5e, the fluorescence emissions of fibrous strips turned from blue to green after incubation with *E. coli*/*pUC19* from 10^2 to 10^5 CFU mL^{-1}. Thus, the fibrous strips indicated potential in the real-time detection of antibiotic-resistant bacteria, which is useful in healthcare or social settings without complex experimental procedures.

Aptamers usually bind target substances *via* non-covalent interactions, and the interactions could be disturbed by environmental pH, temperature and ionic strengths.[39] In the current study, the bacteria-captured fibers were regenerated after incubation in salt solutions, which could unfold the aptamer structure without causing damage.[31] Fig. 5f shows the fluorescence intensities of bacteria captured by the regenerated fibers in the presence of TPE-Cep probes. The aptamer-grafted fibers exhibited bacterial capture ability even after hybridization–denaturation–hybridization for 5 cycles, showing high regeneration ability of the fibrous biosensor.

ROS generation and bacterial killing by TPE-Cep probes

ROS generation involves the photoexcitation of photosensitizers from the ground state to the singlet excited state and then intersystem crossing to the triplet state.[16] Chen *et al.* developed a tetraphenylethene-based pyridinium salt bioprobe, and the AIE feature selectively lit up the cell membrane and produced ROS under room light illumination. ROS could oxidize the substances in the plasma membrane and destroy the integrity.[40] In the current study, the ROS production in the captured bacteria was examined after incubation with nonemissive DCFH-DA, whose fluorescence was turned on at 520 nm after oxidation by ROS.[32] As shown in Fig. 6a, there was no fluorescence emission of DCFH-DA in the presence of bacteria or TPE-Cep probes alone. In addition, the incubation of DCFH-DA in the dark with the bacteria-captured fibers and TPE-Cep probes did not affect the fluorescence emission at 520 nm. However, under room light illumination, strong fluorescence was produced after incubation with the bacteria-captured fibers, indicating efficient ROS production by TPE-Cep probes in the captured bacteria. Similar light-induced ROS-generation properties were confirmed after incubation with different bacterial concentrations (Fig. 6b). The morphologies of bacteria captured on fibers were detected after treatment with the TPE-Cep probes and room light illumination. As shown in Fig. 6c, *E. coli*/*pUC19* captured on fibers exhibited regular smooth bodies and a well-defined border for overlapped bacteria, indicating a healthy state. After light illumination, shrinkage and fusion of bacteria were observed (Fig. 6d), demonstrating the significant destruction of antibiotic-resistant bacteria.[41]

Conclusions

TPE-Cep probes are constructed by linking TPE-OH with cephalosporin molecules, and the hydrolysis of TPE-Cep by β-lactamase results in the release of TPE derivatives and fluorescence turn-on. *E. coli*-specific aptamers are grafted on fibers for selective capture of *E. coli*, and the interaction with bacteria reaches saturation when the graft density of aptamers increases to 0.9 nmol mg^{-1}. In contrast to *S. epidermidis*, *P. aeruginosa* and the antibiotic-susceptible *E. coli* strain, antibiotic-resistant *E. coli*/*pUC19*C captured on fibers showed strong fluorescence emissions after incubation with the TPE-Cep probes. The fluorescence intensity changes could be statistically fitted to an equation for the quantitative analysis of bacteria. Color strips from blue to green are established for a visual readout of *E. coli*/*pUC19*C levels, and the LOD is much lower than those of previous paper substrates. In addition, the antibiotic-resistant bacteria are efficiently destroyed by ROS produced under room light illumination of AIE probes. Thus, this study demonstrates a strategy for selective capture, specific imaging, trace sensing, and photodynamic destruction of antibiotic-resistant bacteria.

Conflicts of interest

There are no conflicts of interest to declare.

Acknowledgements

This work was supported by the National Natural Science Foundation of China (31771034), the Key Research and Development Program of Sichuan Province (2018SZ0348), and the Analytical and Testing Center of Southwest Jiaotong University for SEM analysis.

Notes and references

1 R. A. Blaustein, D. R. Shelton, J. A. S. Van Kessel, J. S. Karns, M. D. Stocker and Y. A. Pachepsky, *Environ. Monit. Assess.*, 2016, **188**, 56.
2 L. Varadi, J. L. Luo, D. E. Hibbs, J. D. Perry, R. J. Anderson, S. Orenga and P. W. Groundwater, *Chem. Soc. Rev.*, 2017, **46**, 4818–4832.
3 N. Drabińska, B. de Lacy Costello, K. Hewett, A. Smart and N. Ratcliffe, *TrAC, Trends Anal. Chem.*, 2019, **115**, 1–12.
4 C. R. Nemr, S. J. Smith, W. Liu, A. H. Mepham, R. M. Mohamadi, M. Labib and S. O. Kelley, *Anal. Chem.*, 2019, **91**, 2847–2853.
5 T. Huang, Y. Zheng, Y. Yan, L. Yang, Y. Yao, J. Zheng, L. Wu, X. Wang, Y. Chen and J. Xing, *Biosens. Bioelectron.*, 2016, **80**, 323–330.
6 B. R. Choi, J. Cho, J. Kim, J. S. Kim, K. Kim and H. Lee, *Adv. Mater. Technol.*, 2019, **4**, 1800375.
7 J. M. Blair, M. A. Webber, A. J. Baylay, D. O. Ogbolu and L. J. Piddock, *Nat. Rev. Microbiol.*, 2015, **13**, 42–51.
8 L. Li, Z. Li, W. Shi, X. Li and H. Ma, *Anal. Chem.*, 2014, **86**, 6115–6120.
9 Q. Shao, Y. Zheng, X. Dong, K. Tang, X. Yan and B. Xing, *Chem. – Eur. J.*, 2013, **19**, 10903–10910.
10 L. Zhai and K.-W. Yang, *Dyes Pigm.*, 2015, **120**, 228–238.

11 A. Almeida, M. A. Faustino and J. P. Tomé, *Future Med. Chem.*, 2015, **7**, 1221–1224.
12 R. Jia, W. Tian, H. Bai, J. Zhang, S. Wang and J. Zhang, *Adv. Healthcare Mater.*, 2019, **8**, 1801591.
13 J. F. Lin, J. Li, A. Gopal, T. Munshi, Y. W. Chu, J. X. Wang, T. T. Liu, B. Shi, X. Chen and L. Yan, *Chem. Commun.*, 2019, **55**, 2656–2659.
14 H. Jin, T. Zhu, X. Huang, M. Sun, H. Li, X. Zhu, M. Liu, Y. Xie, W. Huang and D. Yan, *Biomaterials*, 2019, **211**, 68–80.
15 Y. Zhang, X. Zhao, Y. Li, X. Wang, Q. Wang, H. Lu and L. Zhu, *Dyes Pigm.*, 2019, **165**, 53–57.
16 E. Zhao, Y. Chen, H. Wang, S. Chen, J. W. Lam, C. W. Leung, Y. Hong and B. Z. Tang, *ACS Appl. Mater. Interfaces*, 2015, **7**, 7180–7188.
17 M. C. DeRosa and R. J. Crutchley, *Coord. Chem. Rev.*, 2002, **233**, 351–371.
18 Y. Yuan, G. Feng, W. Qin, B. Z. Tang and B. Liu, *Chem. Commun.*, 2014, **50**, 8757–8760.
19 F. Hu, S. Xu and B. Liu, *Adv. Mater.*, 2018, **30**, 1801350.
20 L. George, A. Müller, B. Röder, V. Santala and A. Efimov, *Dyes Pigm.*, 2017, **147**, 334–342.
21 S.-X. Wang, C. C. Yap, J. He, C. Chen, S. Y. Wong and X. Li, *Nanotechnol. Rev.*, 2016, **5**, 51–73.
22 L. Zhao, Y. Chen, J. Yuan, M. Chen, H. Zhang and X. Li, *ACS Appl. Mater. Interfaces*, 2015, **7**, 5177–5186.
23 J. Chung, J. S. Kang, J. S. Jurng, J. H. Jung and B. C. Kim, *Biosens. Bioelectron.*, 2015, **67**, 303–308.
24 T. Kato, A. Kawaguchi, K. Nagata and K. Hatanaka, *Biochem. Biophys. Res. Commun.*, 2010, **394**, 200–204.
25 R. Hu, R. Ye, J. W. Lam, M. Li, C. W. Leung and B. Z. Tang, *Chem. – Asian J.*, 2013, **8**, 2436–2445.
26 J. Lv, C. Chen, C. Qian, W. Chen, Y. Xiang and J. Zhang, *Sens. Actuators, B*, 2016, **230**, 653–657.
27 L. Zhao, T. Wang, Q. Wu, Y. Liu, Z. Chen and X. Li, *ACS Appl. Mater. Interfaces*, 2017, **9**, 3400–3410.
28 S. J. Lee, R. Tatavarty and M. B. Gu, *Biosens. Bioelectron.*, 2012, **38**, 302–307.
29 B. Zou, Y. Liu, X. Luo, F. Chen, X. Guo and X. Li, *Acta Biomater.*, 2012, **8**, 1576–1585.
30 L. Ying, C. Yin, R. Zhuo, K. Leong, H. Mao, E. Kang and K. Neoh, *Biomacromolecules*, 2003, **4**, 157–165.
31 L. Guo and D.-H. Kim, *Biosens. Bioelectron.*, 2012, **31**, 567–570.
32 D. Y. Lyon, L. Brunet, G. W. Hinkal, M. R. Wiesner and P. J. Alvarez, *Nano Lett.*, 2008, **8**, 1539–1543.
33 H. C. Neu and K. P. Fu, *Antimicrob. Agents Chemother.*, 1978, **14**, 650–655.
34 Y. S. Kim, M. Y. Song, J. Jurng and B. C. Kim, *Anal. Biochem.*, 2013, **436**, 22–28.
35 A. B. Shapiro, *Methods Appl. Fluoresc.*, 2016, **4**, 024002.
36 A. M. King, D. T. King, S. French, E. Brouillette, A. Asli, J. A. N. Alexander, M. Vuckovic, S. N. Maiti, T. R. Parr Jr and E. D. Brown, *ACS Chem. Biol.*, 2016, **11**, 864–868.
37 C. Shen, X. Li, A. Rasooly, L. Guo, K. Zhang and M. Yang, *Biosens. Bioelectron.*, 2016, **85**, 220–225.
38 P. Naik, S. Jaitpal, P. Shetty and D. Paul, *Sens. Actuators, B*, 2019, **291**, 74–80.
39 J.-H. Park, J.-Y. Byun, W.-B. Shim, S. U. Kim and M.-G. Kim, *Biosens. Bioelectron.*, 2015, **73**, 26–31.
40 W. Zhang, Y. Huang, Y. Chen, E. Zhao, Y. Hong, S. Chen, J. W. Lam, Y. Chen, J. Hou and B. Z. Tang, *ACS Appl. Mater. Interfaces*, 2019, **11**, 10567–10577.
41 X. You, H. Ma, Y. Wang, G. Zhang, Q. Peng, L. Liu, S. Wang and D. Zhang, *Chem. – Asian J*, 2017, **12**, 1013–1019.

